

MESOSCALE MOTIONS IN OCEANIC STRATUS AS REVEALED BY SATELLITE DATA ¹

WALTER A. LYONS and TETSUYA FUJITA

Department of the Geophysical Sciences, The University of Chicago, Chicago, Ill.

ABSTRACT

Over maritime areas, meteorological satellite data generally have been used only in the study of synoptic scale systems. However, TIROS 7 pictures of summertime stratus over the northern Pacific, when rectified and combined with mesoscale radiation analyses, give valuable clues regarding the mesoscale dynamics of the lower atmosphere. Radiation data distinguish stratus from middle level cloud layers. Stratus bands, averaging 15 km. wide and oriented 16° to the left of the geostrophic wind, are thought to be related to horizontal roll vortices. Reflectance cross sections across these bands indicate sharp variations in the thickness of the stratus.

Precisely gridded photographs show the relation of marked clear areas in the stratus to the topography of the Aleutian Islands. Only when exceeding a critical size do isolated mountainous islands produce clear wakes. One island appears to be shedding a possible vortex street. A derived model for the flow of the stable air over long mountain ridges in the Aleutians includes such phenomena as upstream blocking, windward slope bolster eddies, and extreme turbulent mixing on the lee slopes causing clear areas to extend over 100 km. downstream. Radiosonde data indicate that the mixed layer downstream is approximately the depth of the obstructing ridge.

1. INTRODUCTION

Studies of fog and stratus over the open ocean have been rare, so it is not surprising that most meteorologists tend to dismiss them as featureless and uninteresting, at least from a dynamical point of view. Yet, there is no reason to suppose that, as with any other cloud form, there are not processes operating to produce patterns and inhomogeneities. In the past 6 yr. meteorological satellite photographs have detected numerous mesoscale stratus and stratocumulus nephosystems over the oceans. Some resemble patterns in laboratory fluid dynamics experiments, such as Bénard cells (Krueger and Fritz [12]), and the closely related stellar and actiniform patterns discussed by Hubert [9]. Bowley et al. [1], Hubert and Krueger [10], and Chopra and Hubert [2] have investigated various patterns in low clouds beneath strong inversions to the lee of islands. From such studies evidence is accumulating which indicates that atmospheric motions may have their peak in the mesoscale, an understanding of which, in all its elusive complexity, is necessary to begin an approach to the solution of the local forecast problem.

The development of precise analysis schemes for satellite photographic and radiometric data now allows more quantitative research not only on synoptic scale systems, but also on mesoscale phenomena over the open ocean. In addition, it is now possible to explore in detail the relationships between cloud patterns and island topography. This paper illustrates how even a single set of

precisely rectified photographs combined with carefully analyzed radiation data and conventional reports can produce significant insights on mesoscale motions like those mentioned below over regions of the globe where they otherwise could not be studied.

The TIROS 7 photographs that will be discussed here picture a vast area of stratus covering the North Pacific in which exists several noticeable patterns, the most striking of which are parallel bandings in the clouds which extend for several hundred kilometers. In this case, the 1000-km. Aleutian Island chain obstructs the flow of fog and stratus. The clear wakes produced by long mountain ridges oriented normal to the flow and by the numerous isolated mountainous islands of different sizes can be used to study how such obstacles disturb the marine atmosphere. One of the islands, moreover, appears to be generating a vortex street.

2. DATA RECTIFICATION FOR MESOSCALE USE

Figures 1A and 1B show TIROS 7 photographs (frames 6 and 8, pass 735, Aug. 8, 1963) over the northern Pacific Ocean in the vicinity of the Aleutian Islands, with 1° lat. and long. lines superimposed. The details of the method of rectification used here, which has an accuracy of better than 0.1° of lat. near the satellite subpoint (SP) and is sufficient to be useful for research on the mesoscale, have been presented by Fujita [5]. To facilitate the visualization and comparison of the cloud and topographic features, a sketch (fig. 2) including an outline of the Aleutian Islands was made. The numbers are the maximum elevations above sea level (in meters) of each of the islands

¹ This research has been partially supported by the Environmental Science Services Administration under grant Cwb WBG-34.

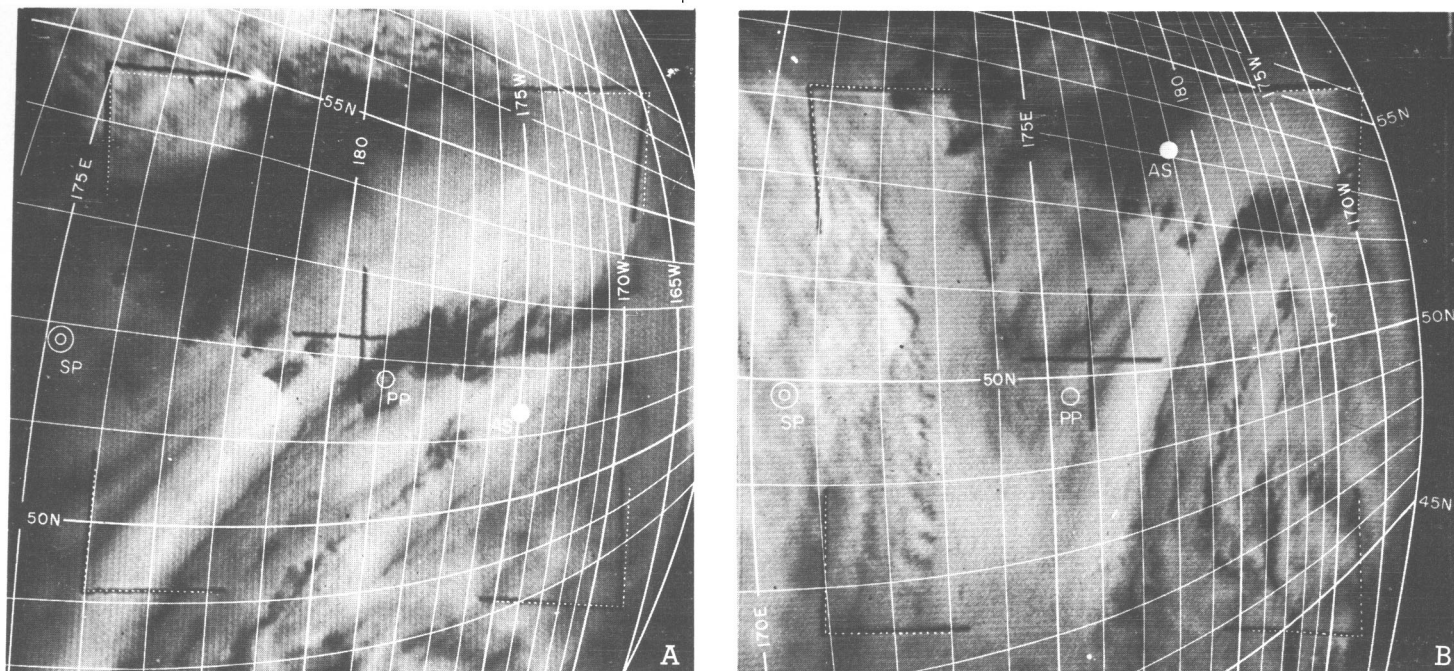


FIGURE 1.—(A) Precisely gridded satellite photograph showing clear wakes in stratus lee of the Aleutians, and, to the south, banded stratus (TIROS 7, pass 735, frame 6T, 0320.5 GMT, Aug. 8, 1963). Photogrammetric data: satellite height, 628 km.; exposure subpoint (SP), 51.8°N., 175.1°E.; exposure principal point (PP), 51.7°N., 174.0°W.; tilt, 33.3°; exposure antisolar point (AS), 51.4°N., 175.0°W. (B) The leading edge of an extensive area of altocumulus casting shadows on the stratus below along 172–173°E. (TIROS 7, pass 735, frame 8T, 0319.0 GMT, Aug. 8, 1963). Photogrammetric data: satellite height, 628 km.; exposure subpoint, 49.8°N., 170.5°E.; exposure principal point, 49.7°N., 175.4°E.; tilt, 30.1°; exposure antisolar point, 53.1°N., 173.9°E.

and will be used for identification. Other information in figure 2 pertains to the various cloud features to be discussed.

Even though the exact positions of the cloud elements have been fixed, the difficulty of determining their type and altitude remains. Recourse to the few scattered surface reports would be insufficient to establish the structure of a multilayered cloud system. The channel 2(8–12 μ) “water vapor window” medium resolution radiometer of TIROS 7 is capable of estimating the altitude of the tops of cloud layers of the horizontal scale of several tens of kilometers by inference from their effective blackbody temperatures. Fujita [7] has developed a “scanning-printer” which uses the original analog telemetry recording and produces an analysis for any of the five radiometer channels having continuous gradients of radiation values and a rectification accuracy comparable to the photographs. Figure 3 shows the equivalent blackbody temperatures of the viewed surface (cloud top or sea surface) over our area as derived from channel 2. A representative radiometer scan line and scan spot (isopleths of returned power) are included. While no correction for water vapor attenuation was applied, the extreme dryness of the atmosphere in this case (motorboating was observed from 940 mb. up) indicates that the temperatures shown are probably within 1 or 2°C. of the actual. Note the correspondence of an observed sea

surface temperature with that measured by the satellite. The sharp radiative temperature gradients clearly delineate two distinct cloud layers, the warm regions associated with a very low level cloud (stratus) and the areas colder than about -4°C . (heavy stipple) representing altocumulus. Distinguishing low from middle clouds is important, since it suggests that the clear breaks in the stratus lee of the islands are the result of motions much shallower than lee waves, which often extend through the entire depth of the troposphere. Note that undisturbed altocumulus actually obscured portions of the clear wakes from Attu (640 m.) and Agattu (633 m.).

A surface sectional map interpolated to 0300 GMT with three aviation weather reports available from the islands is shown in figure 4. A large High (1031 mb.) was centered at 175°W., 48°N., with a ridge extending from southern Alaska southwestward to 35°N. Ship reports and time sections of surface data from the islands (not shown) indicate that dense fog and low stratus (base about 30 m.) beneath a strong, low level inversion (7.5°C./150 m.) in the southwesterly flow covered a huge area of the northern Pacific. Rain began falling at Attu (640 m.) at 0700 GMT as the line of altocumulus at 173°E., which was running ahead of a weak surface cold front along the 165°E. meridian, passed overhead. It might be noted that the pronounced shadows cast by the altocumulus line onto the bright stratus tops provide an additional

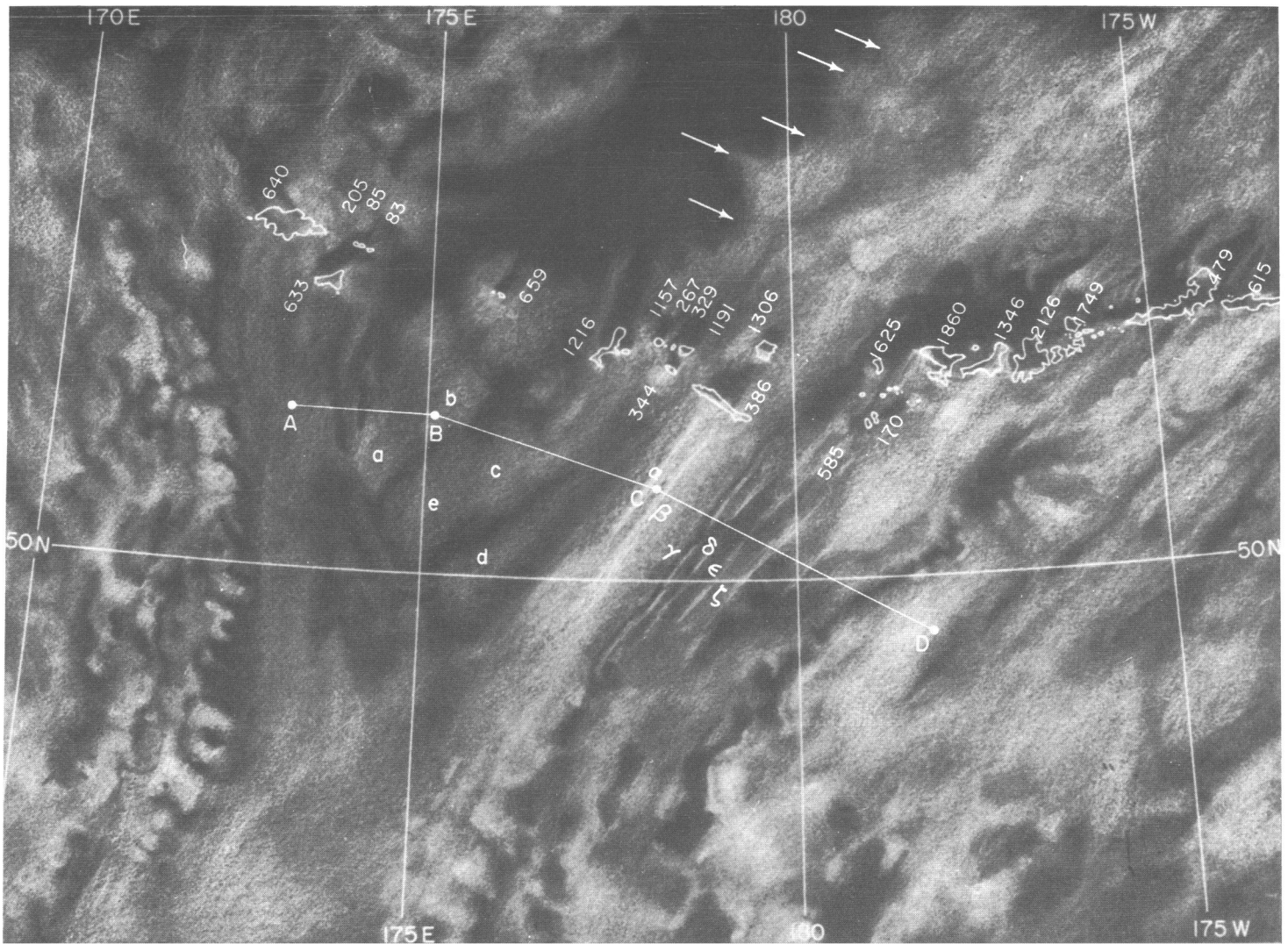


FIGURE 2.—Cloud sketch made from figures 1A and 1B. Numbers indicate the maximum heights (m.) of the islands in the Aleutian chain. Letters α through ζ mark some of the more pronounced bands and “a” through “e” label several block-like patterns in the stratus. The reflectance calculations of figure 5 were made for cut ABCD. Arrows point to the probable vortex street shed by Kiska (1216 m.).

way to distinguish cloud layers. One can verify that the dark markings are indeed shadows and not holes in the stratus since the vectors connecting the clouds and their assumed shadows all point towards the antisolar point (AS) (where the shadow of the satellite would be visible if large enough) (Fujita [6]) as shown in figure 1B.

3. THE STRATUS PHYSIOGNOMY OVER OPEN OCEAN

As figures 1 and 2 show, the stratus hardly appears amorphous. Several features can be discerned, particularly a family of parallel cloud bands (500 km. in length and lettered α through ζ) south of the islands. Widger, Sherr, and Rogers [21] speculate that such streaking in oceanic stratus arises from differential advection of cloud and clear air by parallel wind bands of differing velocities. A more likely explanation is stationary (or slowly moving) parallel, horizontal roll vortices of sufficient vertical extent to

cause cloud banding. These “large eddies,” i.e., larger than those of the normal turbulent spectra in the frictional layer, within a turbulent, adiabatic boundary layer appear to require an inflection point (I) in the boundary layer wind profile as implied by the profile in figure 11 (Faller [3]). To estimate the variations in cloud thickness in these bands figure 5 was prepared. The fine structure of stratus brightness along cut ABCD in figure 2, based on an arbitrary gray scale from 1 to 10, is shown. These values are in turn converted into units of reflected solar radiation (W) by comparison of the gray scale with the readings in the channel 5 (0.55–0.75 μ) analysis (not shown) in areas where the radiometer scan spot viewed a relatively uniform cloud or water surface. From the solar zenith angle of 49°, the satellite zenith angle of 20°, the effective solar constant for the channel 5 filter of 117.13 watts/m.², and a mean effective atmospheric transmission coefficient of 0.80, the average reflected radiation (\bar{W}^*) reaching the satellite from a cloud top acting as a perfect

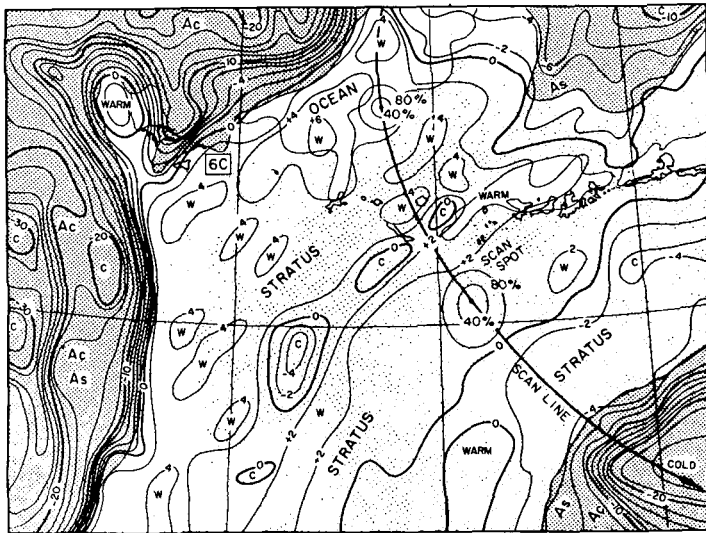


FIGURE 3.—2°C. isotherms of cloud top or sea surface effective blackbody temperature from the channel 2 (8–12 μ) medium resolution radiometer measurements simultaneous with the photographs in figures 1A and 1B. The altocumulus (Ac) layer (heavy stipple) is roughly delineated from the stratus (light stipple) by the –4°C. isotherm. A typical scan line and scan spots (isopleths of percentage of power return) are shown. Shemya's (83 m.) sea surface temperature (box) compares well with the value of the radiometer in the cloud free area northeast of the island.

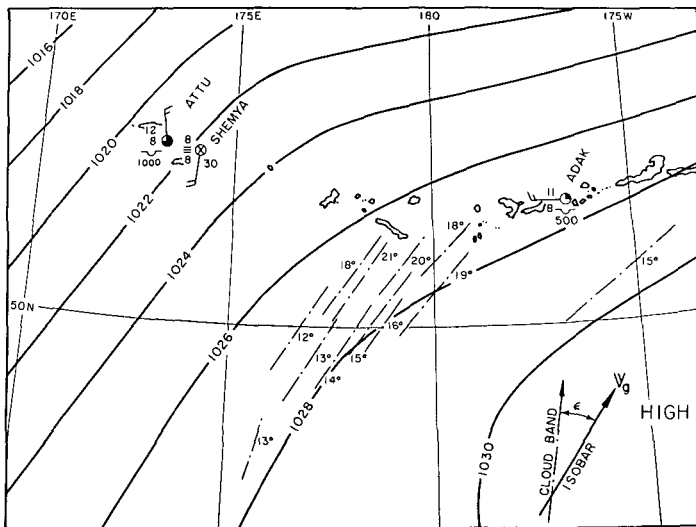


FIGURE 4.—Surface synoptic chart interpolated to 0300 GMT, Aug. 8, 1963, with full wind barbs equal to 5 m./sec. and cloud bases given in meters. Cloud band orientations are indicated by the deflection angle ϵ which they make with the surface isobars.

diffuse reflector is calculated to be 56.6 watts/m.² Therefore, the cloud reflectance (W/\bar{W}^*) along cut ABCD can be computed and in turn approximately related to the stratus thickness by using the total albedo measurements of Neiberger [16] (right hand side of figure 5). The undulations in the stratus thickness are calculated to be as great as 170 m. (between bands β and γ) which is the

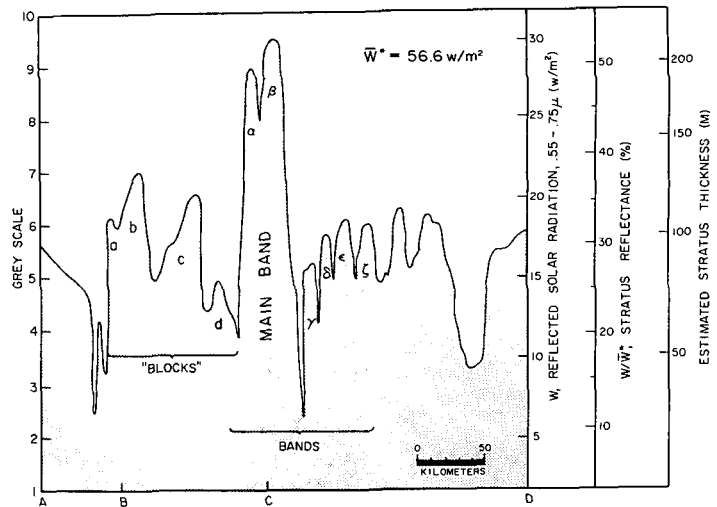


FIGURE 5.—Cloud brightness based upon gray scale of 1 to 10 along cut ABCD in figure 2. These values are converted, on the three abscissas on the right, into reflected solar radiation (W) from the channel 5 (0.55–0.75 μ) analysis, cloud reflectance (W/\bar{W}^*), and estimated cloud thickness, which is seen to vary by as much as 170 m., averaging about 50 m.

depth of the stratus estimated from the 0000 GMT Shemya (83 m.) sounding, and which also fits the fact that the ocean surface appears visible in this region of descending motion.

Faller [3] states that in the atmosphere the band spacing $L=0.2U/\sin \Phi$, where L is in kilometers, U is the wind speed above the boundary layer in meters per second, and Φ is the latitude. If we take $U=15$ m./sec., the calculated L is 3.8 km. The average value of L from figure 5 is 14 km. Faller, however, refers to a quasi-adiabatic boundary layer. While the effects of thermal stratification (see fig. 11) still remain unknown, the great thermal stability here may have forced these eddies to become oblate resulting in the observed four-fold increase in L over the expected value. Also, by analogy with Faller's rotating tank experiments, it is indicated that the bands (in the Northern Hemisphere) should be oriented to the left of the geostrophic wind by an angle ϵ , which ranges between 10° and 17° and averages 14°. In figure 4, the more pronounced bands are indicated by dashed lines, and observed values of ϵ are measured to range from 12° to 21°, with an average of 16°, an acceptable comparison. Also, the most prominent of the stratus bands shows its own internal striations (α and β) and narrower, less intense bands are present to the right (γ through ζ). Faller's laboratory experiments also showed strikingly similar structures in which a broad striated band, often with a sharp edge, was paralleled by weaker, less pronounced streaks.

Ogata and Tamura [17] presented a summary of observations taken at ship *Extra* (39°N., 153°E.), which notes that fog often drifts in masses or blocks of between 15- and 90-km. diameter. The shallow stratus and fog in figure 2 seems to have a similar block-like structure

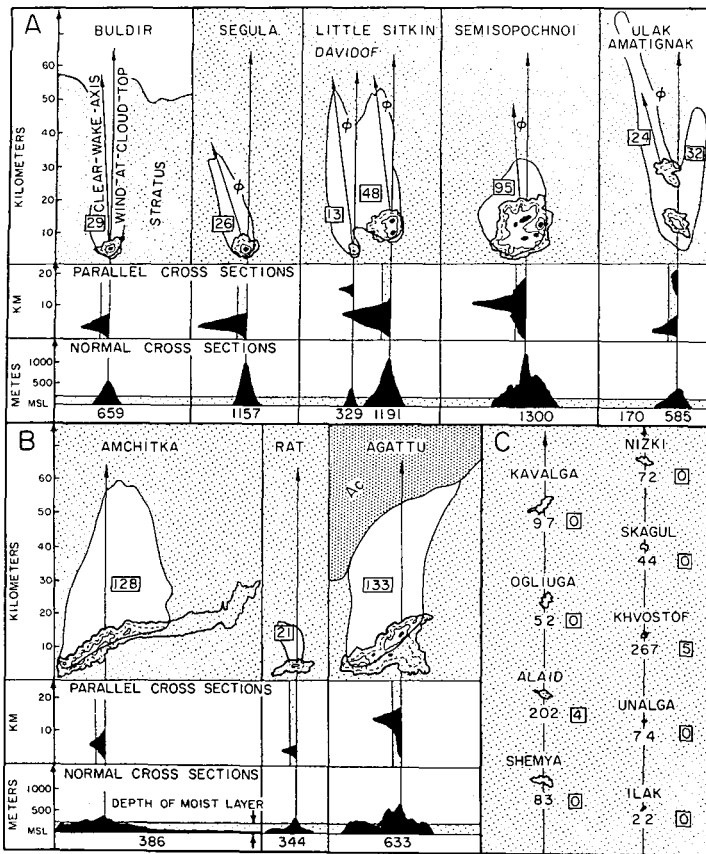


FIGURE 6.—(A) Wakes lee of cone-shaped, isolated mountainous islands. Island cross sections are made both parallel and normal to the cloud top (200 m.) wind vector (vertical line) passing through the highest elevation of the island, which is indicated beneath the sections. Calculated Reynolds numbers for each island are shown in boxes. ϕ is the angle of deviation of the clear wake axis to the left of the 200-m. wind. The 100-m. (dashed) and 200-m. (solid) contours are shown, and elevations greater than 600 m. are painted black. (B) Wakes lee of small islands with elipsoidal profiles. (C) Islands producing no visible wakes.

(labeled "a" through "e") with an average dimension parallel to the winds of about 90 km. However, again by analogy to Faller's laboratory results, stratus bands should move normal to the wind at $0.1 U$. Therefore, for a U of 15 m./sec. it would take 1.8 hr. for 10-km.-wide cloud bands to pass a stationary observer who, assuming that the stratus was moving with the wind, could interpret them as roughly 100-km.-long "blocks" of stratus and fog.

4. WAKES TO THE LEE OF ISOLATED ISLANDS

For this study, extreme care was taken to maximize the rectification accuracy of pictures in the vicinity of the islands in order to detail the relationships between the topography of an island and its wake. Twenty isolated islands were divided into four categories: those almost conical in shape (fig. 6A), those more resembling ellipsoids yet sufficiently small to allow flow around them (fig. 6B), those producing no wakes (fig. 6C), and Kiska (fig. 9B),

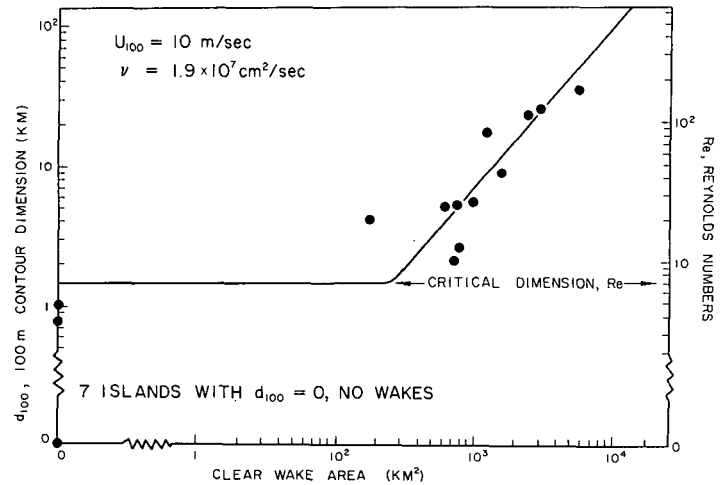


FIGURE 7.—The length of the 100-m. elevation contour normal to the wind (d_{100}) plotted versus the clear wake area for 20 isolated islands. The right hand ordinate gives the computed Reynolds number for each island. The critical d_{100} for clear wake formation in this case appears to be slightly greater than 1.0 km., equivalent to a Reynolds number of about 7.

treated separately below. Cross sections of topography both normal and parallel to the wind at stratus top level (200 m.) and the depth of the stratus and fog layer are shown for the islands with wakes. Clear wakes can result from one of three basic mechanisms: 1) horizontal flow of stratus and fog about the obstacle, 2) vertical mixing of moist and dry layers on the downwind slope by intense turbulence induced by the island, and 3) evaporation of liquid water as a result of heating of the air by contact with the surface of the island. The last would seem to be of minor importance here due to the overcast and rather low sun elevation (41°). The fact that on all islands, notably Amchitka (386 m.) and Rat (344 m.), wakes only occur downstream of the segments rising above 100-m. level points toward a dynamic origin. Choosing between the first and second mechanism is not so easy, and undoubtedly both occur simultaneously on all the islands in proportions varying with the size of the island, particularly its cross wind diameter.

A plot of the length of the 100-m. contour normal to the flow (d_{100}) versus the area of the clear wake for the 20 isolated islands is shown in figure 7 and reveals an apparent critical obstacle dimension below which a clear wake will not form. Above this size, wake areas are directly proportional to the width of the island beneath the stratus top. The islands with wakes penetrate well above the inversion level and present shapes to the low level saturated flow not at all unlike extended circular or elliptic cylinders. Indeed, the wake patterns bear a noticeable similarity to those seen in laboratory experiments with two dimensional cylinders, where wakes develop downstream of bluff bodies only above a certain critical value of the Reynolds number (R_e) defined as

$$R_e = U_0 d / \nu \quad (1)$$

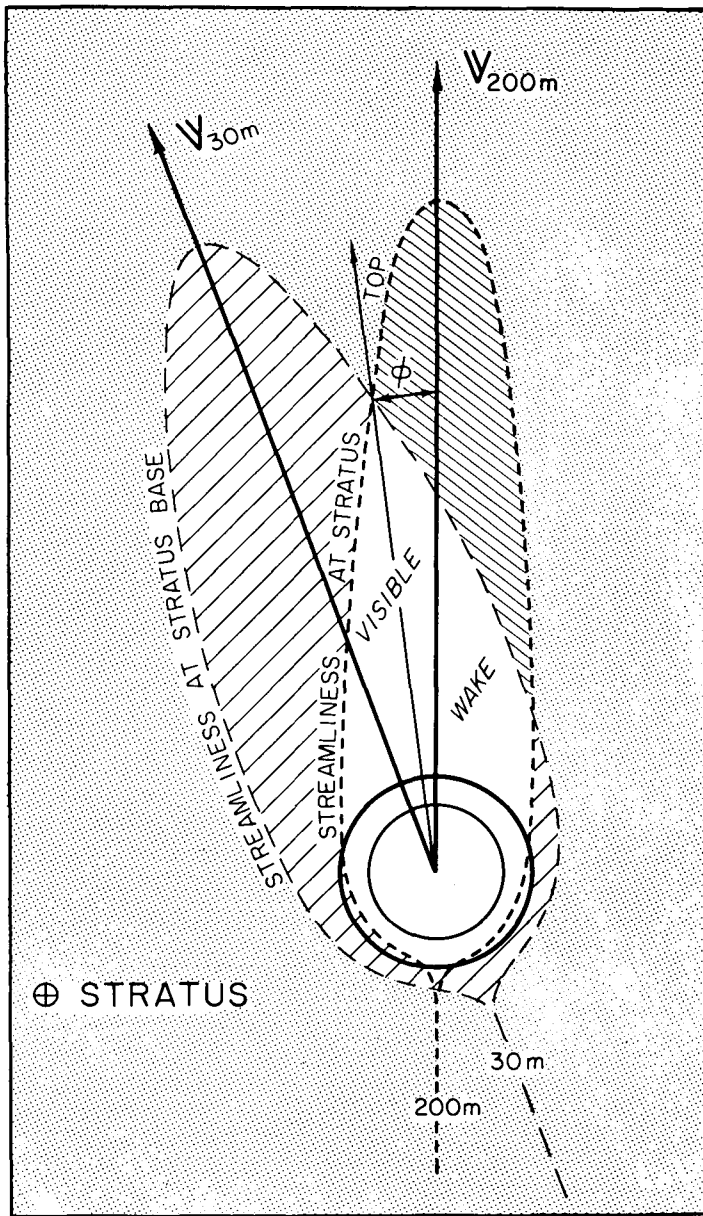


FIGURE 8.—The visible wake oriented by an angle ϕ to the left of the cloud top wind direction as a result of wind direction shear in the stratus layer. This is illustrated by the superposition of the assumed wake flow streamlines at the cloud top (200 m.) and at the cloud base (30 m.), based on the 22° veering of the wind in the 0000 GMT, Aug. 8, 1963, Shemya sounding.

where U_0 is the stream velocity, d a characteristic cross stream dimension of the object, and ν is the kinematic, or for an atmospheric case, eddy viscosity. Using a value for ν of 1.9×10^7 cm.²/sec. (computed below) and a U_0 of 10 m./sec. (the wind speed at the 100-mb. level), Reynolds numbers are computed for each island using d_{100} as the cross stream dimension of the obstacle. The computed values of R_e are shown in boxes in figures 6 and 9 and appear to be within an order of magnitude of those giving similar streamline patterns in laboratory experiments. The critical R_e for clear wake formation appears to be slightly greater than 5, considering that

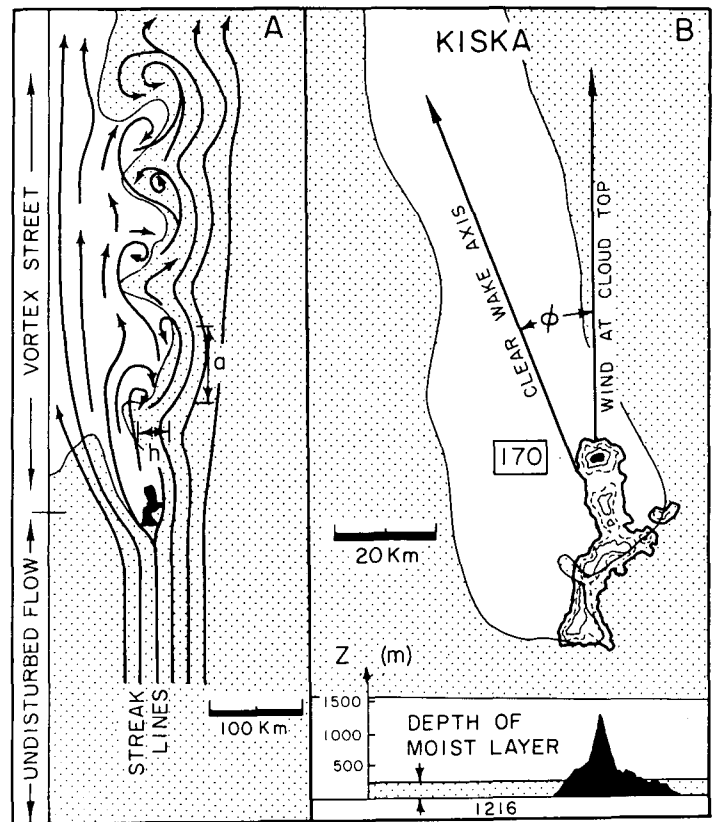


FIGURE 9.—(A) Hypothesized streak lines of the Kármán vortex street originating on Kiska that would cause the observed perturbations in the stratus and fog bank upstream. Characteristic dimensions a and h are shown. (B) The detail of the wake from Kiska. Stratus flares outward along the 100–150-m. contour and only crosses the island where there is a break in the ridge.

Khvostof (267 m.) has a d_{100} of 1.0 km. ($R_e=5$), yet no clear wake, while Davidof ($R_e=13$) does. For islands smaller than this, horizontal air motions probably approximate potential flow.

The tendency of some of the wakes to deviate by an angle ϕ as much as 25° to the left of the 200-m. wind is the result primarily of directional shear within the stratus layer. The 0000 GMT sounding at Shemya (83 m.) showed a 50° veer in the lowest 500 m. As shown in figure 8, the 22° direction change within the cloud layer results in a visible wake having its apparent axis deviated 15° to 20° to the left of the banding. This is obtained by superimposing assumed flow patterns about a conical island at the 30-m. (stratus base) and the 200-m. (stratus top) levels. Variations in ϕ can also result from local variations in stratus thickness.

Although the motion about these small islands is essentially horizontal, our assumption that the heat input into the air stream from the surface of the island is rather small leads us to conclude that there must be some downward transport of drier air from above the inversion into the clear wake in order to evaporate the liquid water. This may be explainable by the observation of Scorer [19] that air flowing about a conical hill can separate from the

boundary layer of the hill, curve upwards a small distance, and then proceed down the lee slope. This motion would probably allow enough dry air to be incorporated into the wake to make it clear.

5. A VORTEX STREET

The wake of Kiska (1216 m.), the island with the largest $R_e(170)$, is the most pronounced from any of the islands and extends 125 km. downstream. The wind impinged upon the upwind slopes and appeared to flare outwards to both sides along the 100–150-m. contours, with a small patch of stratus extruded across the island through a pass where the elevation drops to about 125 m. (fig. 9B). North of the wake, extending an additional 350 km. upstream, the edge of the stratus and fog bank had a noticeably scalloped appearance as indicated by the arrows in figure 2. When visible farther west on pass 721, 24 hr. earlier, the same cloud bank appeared quite smooth, and it seems likely that these perturbations may be dynamically significant. Chopra and Hubert [2] studied mesoscale eddies in stratocumulus in the wake of Madeira Island beneath a strong inversion and concluded that an atmospheric analog to the laboratory Kármán vortex street exists. In figure 9A, streak lines are drawn for the Kármán vortex street which would have produced the observed perturbations in the formerly straightedged cloud bank.

Without going into detail, we will use essentially the approach of Chopra and Hubert to calculate several characteristic parameters for the Kiska case in order to compare them with those obtained for Madeira. In a vortex street, the ratio of the average lateral spacing of the vortices (\bar{h}) to the average longitudinal spacing (\bar{a}) should fall within the range $0.28 \leq (\bar{h}/\bar{a}) \leq 0.52$, the lower values pertaining to idealized conditions and circular cylinders. The nondimensional drag coefficient C_D can be approximated by the ratio (\bar{h}/d) , and for irregularly shaped bodies is probably somewhere between 1.5 and 2.0, or slightly larger. Lin [13] has established a dimensionless parameter β which is an inherent property of a stable vortex street. Laboratory estimates of β in the presence of vortex streets for flow about circular cylinders range from 1.0×10^{-3} to 2.5×10^{-3} . The Reynolds number can be calculated using

$$R_e = dN/\beta U_0, \quad (2)$$

where N is defined as the rate of shedding of vortex pairs. The reciprocal of N , the time interval T between the shedding of vortices of the same sign, can be found by

$$T = 1/N = 4\bar{a}/3U_0 \quad (3)$$

if one assumes that the eddies travel downstream at 0.75 of the mean current U_0 . T_{ive} is defined as the age of the farthest visible eddy at a distance l downstream.

A most useful by-product of the above approach is that the eddy viscosity can be computed by combining

TABLE 1.—Observed or estimated input values

Island	\bar{a}	\bar{h}	d_{100}	U_0	l	β
Madeira.....	190 km.	83 km.	43 km.	10 m./sec.	540 km.	1.75×10^{-3}
Kiska.....	85 km.	25 km.	18 km.	10 m./sec.	475 km.	1.75×10^{-3}

TABLE 2.—Characteristic parameter

Island	\bar{h}/\bar{a}	C_D	R_e	ν	T	T_{ive}
Madeira.....	0.43	1.95	98	4.2×10^7 cm. ² /sec.	7.0 hr.	20.0 hr.
Kiska.....	0.30	1.42	100	1.9×10^7 cm. ² /sec.	2.6 hr.	14.7 hr.

equations (1), (2), and (3) to obtain the relations

$$\nu = \beta U_0^2 / N = 4\beta U_0 \bar{a} / 3,$$

which assumes that the vertical momentum transfer is negligible. We will assume that true vortex streets existed for both cases and take a mean value of β of 1.75×10^{-3} .

Table 1 compares the observed or estimated values used in the computation of six characteristic parameters for the two islands and their vortex streets as shown in table 2. Since the two sets of values compare quite closely it does not seem rash to speculate that Kiska is shedding a Kármán vortex street. Vortices may perhaps have been produced by some smaller islands, but these would have been embedded within the stratus overcast and the TIROS camera most likely could not have resolved the pattern.

The eddy viscosity is perhaps one of the most difficult physical variables of the atmosphere to evaluate. Chopra and Hubert assign no more than an order of magnitude reliability to their estimate of about 4.2×10^7 cm.²/sec. and quote Heffter's [8] computations of ν based on all available data, which indicated a range in values from 10^5 up to 10^9 cm.²/sec. Our estimate of 1.9×10^7 cm.²/sec. for the Kiska case is surprisingly close. A pertinent reference may be Voskresensky and Matveev [22] who concluded from 78 aircraft turbulence measurements in summertime stratus at the 100-m. level over the ice-free Arctic Ocean that ν rarely reached above 10^6 cm.²/sec. and most frequently was 5×10^5 cm.²/sec. The discrepancy of two orders of magnitude between the above values of ν may represent real variations, the effect of eddy anisotropy, or indicate that equating values of β from the laboratory to the atmosphere is not entirely justified. Also, the eddy visible farthest downstream was at least 14 hr. old, supporting Chopra and Hubert's reconsideration of Hubert and Krueger's [10] statement that mechanical eddies can not persist for more than 8 hr. due to frictional loss of eddy momentum to the sea surface.

6. WAKES TO THE LEE OF LONG RIDGES

The Aleutians east of 180° , as indicated by their cross sections (fig. 10A), present an extended horizontal barrier

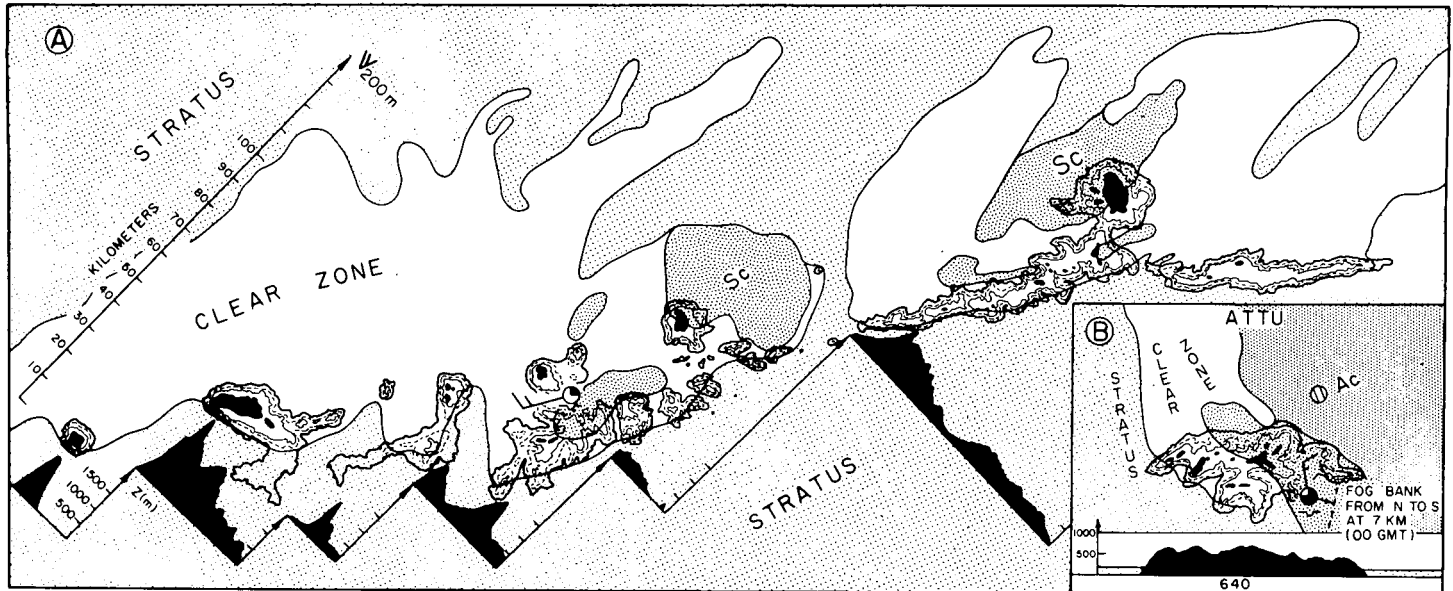


FIGURE 10.—(A) Clear zone produced by the continuous chain of islands east of 180° . The 0300 GMT Adak surface observation is entered. Patches of stratocumulus (heavy stipple) rest on top of the shallower portions of the mixed layer. (B) Inset shows Attu (640 m.), large enough to be considered an extended ridge, with its downstream clear zone partially covered by altocumulus and scattered stratocumulus on top the mixed layer. North-northwest winds and the absence of fog and stratus along the south shore of the island illustrate the effect of the windward slope bolster eddy.

to the low level winds. The air beneath the inversion must be forced up and over the long ridges since substantial horizontal flow about the islands becomes difficult for large cross current widths. The model of air motions in the vicinity of these ridges presented in figure 11 will be used to explain the various features seen in the satellite photographs.

The clear zone extending as much as 120 km. from the island chain does not contain the wave-like corrugations with spacings of from 5 to 25 km. normally expected from the "classical" atmospheric lee wave. These wakes, on the contrary, appear to be the result of strong turbulent mixing of the shallow moist layer with dry air from above. Long [15] points out that linearization of the differential equations eliminates the simulation of jumps and other shock phenomena from theoretical studies of lee effects. His experiments with stratified fluids (Long [14]) indicated that at moderate Froude numbers (a wind speed of about 20 m./sec.) hydraulic jumps may occur lee of mountains. Unless the tropospheric inversion is quite high and the barrier low (a 300-m. relief is sufficient for lee waves), we should expect the presence of surges, jumps or bores, not low amplitude, sinusoidal waves. Long concluded that this should be particularly true for very strong atmospheric inversions.

His experiments using a fluid with a sharp density gradient often showed a turbulent jump with rotor-like vortices in the lee of the obstacle. Furthermore, while the existence of a statically stable layer lying near the crest of a mountain range oriented within 30° of the normal to a rather strong wind is a necessary condition for lee waves,

Scorer's [18] theory would indicate this is not sufficient. It seems important that the wind show little directional change but increasing speed with height through a deep layer, which was clearly not the case here. Also, since the mere oscillation of the stable layer about an equilibrium level in a simple lee wave is not *per se* accompanied by great turbulence, observational evidence is needed of a far more turbulent type of lee motion able to destroy a moist layer lying close to the surface. Förchtgott [4] discovered that when stable air moves roughly perpendicular to a ridge the lee effect depends primarily upon the low level wind profile. When strong winds are confined to a layer approximately the depth of the hill as in Shemya's wind profile, there occurred "rotor-streaming," i.e., a rapid downrushing current on the lee slopes accompanied by extreme turbulence and one or two large, quasi-stationary horizontal vortices about the length of the obstacle downstream. Such a motion is suspected in this case.

Both surface and upper air data support the above conclusion. At 0500 GMT, the surface winds at Adak shifted to strong and directly downslope, due apparently to either an intensification or a change in location of the downrushing current on the lee side. The wind shift was accompanied by a 0.5-mb. pressure drop in less than 1 hr., explainable as a dynamic low pressure which would help induce any surface return flow present beneath the rotors. Most significant, however, is that the surface dewpoint fell abruptly from 6.5 to 1.5°C., lower than anywhere in the entire northern Pacific Ocean, and remained such for the duration of the downslope winds.

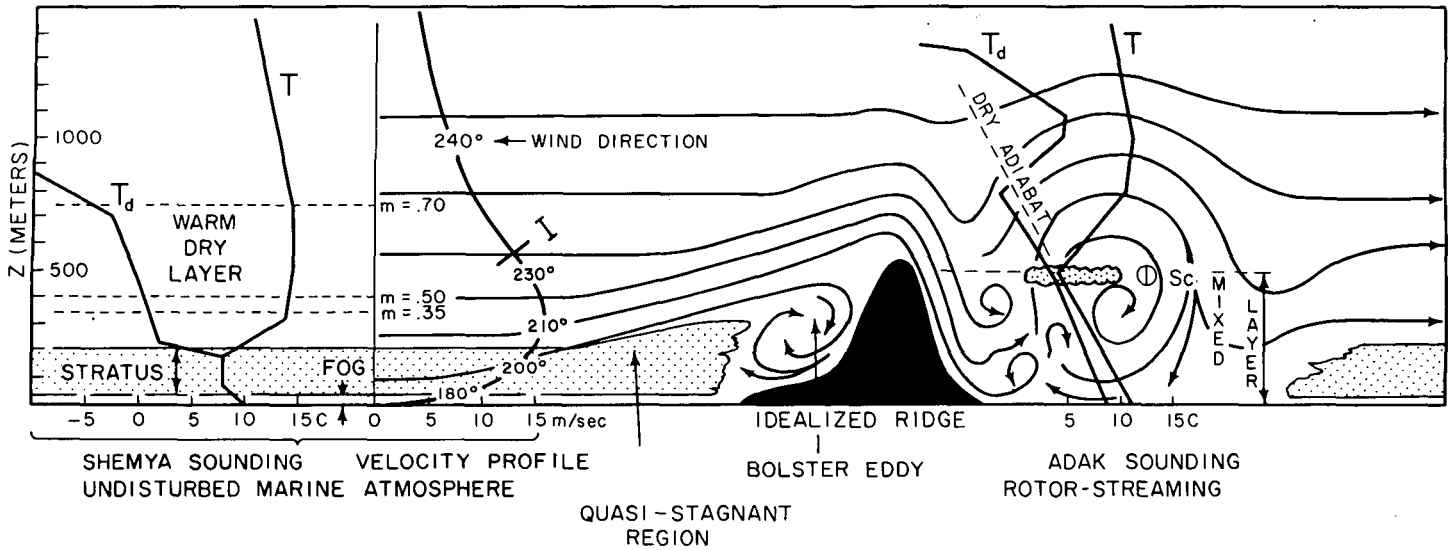


FIGURE 11.—Model of flow of a stable airstream with a pronounced low level wind maximum over an extended mountain ridge. The 0000 GMT, Aug. 8, 1963, Shemya and Adak soundings represent initial and disturbed conditions respectively. Tops of the mixed layer for several values of M are shown. I marks the inflection point in the boundary layer wind profile. Upstream, the stratus depth is at first increased by the blocking effect of the island, but, closer to the coast, is destroyed by the bolster eddy circulation. The extreme turbulence in the rotor-streaming region on the lee slope produces a cloud-free mixed layer downstream approximately the height of the obstacle.

This was the result of dry air from about the 300-m. level managing to penetrate all the way to the surface during this period.

The only two upper air stations in the Aleutians are fortuitously positioned to give further credance to our model. Shemya (83 m.) is a low, exposed island giving readings representative of the free and undisturbed conditions over the entire area of study due to the marked horizontal homogeneity of the air mass. A shallow (50 m.) adiabatic layer is present at the surface beneath the inversion over the open ocean. Adak (2126 m.) is located in the clear wake of the island 8 km. downstream of its 400-m.-high mountain ridge. As shown in figure 11, the depth of the adiabatic layer has jumped to 500 m. on Adak's downwind slope, which, along with the more evenly distributed moisture, indicates extensive mixing. To obtain a rough estimate of the magnitude of the "vertical entrainment" necessary to produce the observed changes, the following procedure was adopted. A moist layer 200 m. deep was considered to have a mean potential temperature $\bar{\nu}'$, a mean saturation mixing ratio \bar{r}' , and a mean liquid water content \bar{l}' , or mean liquid water mixing ratio $\bar{\chi}'$. Liquid water content of the stratus was estimated as 0.30 gm./m.³ and of the fog as 0.10 gm./m.³ Complete adiabatic mixing of the dry and moist layers was assumed, with the effects of cooling and addition of water vapor to the air from the evaporation of cloud droplets taken into account. If M is defined as the percentage of air in the final mixed layer which originated from above the stratus top, then the final potential temperature $\theta^*(M)$, uniform mixing ratio $r^*(M)$, and relative humidity $R^*(M, z)$ in the mixed

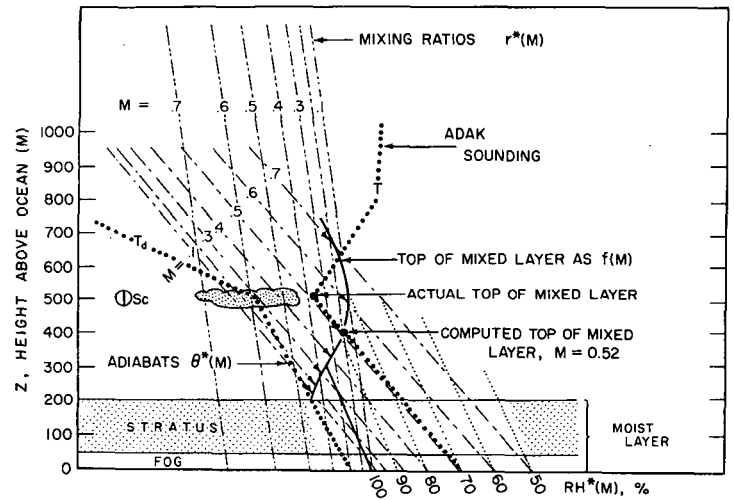


FIGURE 12.—Family of adiabats (dashed lines) and constant mixing ratio (double-dashed lines) for values of M from 0.0 to 0.7. Proceeding down an adiabat, the height of the mixed layer is found by its intersection with the heavy, curved line and the relative humidity in the mixed layer by its intersection with the dotted line. The 0000 GMT Adak sounding indicated $M=0.52$. The observed top of the adiabatic layer was about 100 m. deeper than the calculated.

layer are calculated by

$$\begin{aligned} \theta^*(M) &= M\bar{\theta}(M) + (1-M)(\bar{\theta}' + \bar{l}'L/c_p) \\ r^*(M) &= M\bar{r}(M) + (1-M)(\bar{r}_s' + \bar{\chi}') \\ R^*(M, z) &= r^*(M)/r_{s^*}(M, z) \end{aligned}$$

where L is the latent heat of evaporation, c_p the specific heat of moist air at constant pressure, z the height above

the ocean, and $\bar{\theta}(M)$ and $r(M)$ the mean values of the potential temperature and mixing ratio of the dry air involved in the mixing. All initial values are from the 0000 GMT Shemya sounding. M was varied from 0.0 to 0.7, and the resulting family of adiabats and constant mixing ratio (dashed and double-dashed lines) and the relative humidities in the mixed layer (dotted lines) are combined with the 0000 GMT Adak sounding (heavy dotted lines) in figure 12. As one proceeds down the adiabat for a given value of M , the relative humidities can be picked off as a function of altitude. The 100 percent relative humidity line (heavy straight) indicates the base of the saturated layer for various values of M whereas the heavy curved line denotes the top of the mixed layer as a function of M . Their intersection indicates that an M of 0.35 was needed to evaporate all the liquid water. The potential temperature of the Adak sounding indicated that mixing continued up to about $M=0.52$. This means that the warm dry air from 200 to 400 m. was substantially mixed with the stratus and fog below, agreeing with the proposed streamline pattern for flow over the ridge. While the mixing ratio of the sounding was not constant with altitude since 100 percent mixing is improbable, the mean value corresponds very closely to that for an M of 0.50. The relative humidity at the top of the mixed layer for $M=0.50$ was calculated to be 87 percent. The fact that there were scattered patches of stratocumulus at 500 m. north of the lee slopes (Adak aviation reports) means that the degree of mixing varied along the island chain and was occasionally small enough to allow a thin cloud layer to remain at the top of the mixed layer.

Several upstream phenomena also seemed to be present. Long's [15] experiments and the calculations of Kao [11] have demonstrated that a quasi-stagnant layer approximately the height of the obstacle can exist for a considerable distance upstream in a stably stratified fluid. In the original photographs, crescent-shaped regions can be seen extending a few kilometers upstream of several of the islands. There the stratus appeared brighter than that surrounding it, indicating a partial blocking was occurring. As the air "piled up" in the quasi-stagnant zone, the inversion surface was lifted somewhat and the deeper stratus layer was manifested by its higher reflectance. However, it should be noted that a portion of the incident airstream must descend down the windward slopes of many of the islands. On Attu (640 m.) north-northwest winds of 7 m./sec. were recorded at the base of the 400-m. ridge which runs northeast through southwest of the station (see fig. 10B). As indicated by the remarks on the 0000 GMT Attu aviation report, the downward incursion of dry, potentially warmer air was actually destroying the stratus upwind of most of the islands. In the satellite photographs, this was most noticeable along the continuous chain of islands and at Amatignak (570 m.), where clearing began 3 km. upstream of the steep windward cliffs of the islands (fig. 6A). This feature, called a "bolster eddy" by Scorer [20], is incorporated into the model in figure 11.

7. CONCLUSIONS AND DISCUSSION

Precisely analyzed TIROS 7 data have shown the usefulness of the meteorological satellite in exploring the mesoscale dynamics of the marine boundary layer, both over the open ocean and as it is disturbed by island obstacles. It seems probable that longitudinal roll vortices existed in the lowest 1 km., though the relationship between their rather large horizontal spacing and the very high stability of the layer must be further investigated.

There seems, indeed, to be some justification in comparing flow around isolated mountainous islands with that about two dimensional cylinders in the laboratory. However, other phenomena beside simple wake formation may be possible and which will be best studied by pictures of the quality obtained on manned orbital missions. Islands at high latitudes, like the Aleutians, cause mesoscale perturbations in the low level airflow during both the warm (stable) and cold (unstable) seasons. Regular lee wave patterns, vortex streets, and blocking and dissipation effects, like those discussed here, can and should be studied under the vast range of thermal stabilities which are not found in the vicinity of islands in middle and low latitudes. Here, the phenomenon of rotor-streaming, which occurs when very stable air with a pronounced low level wind maximum is forced over a mountain ridge, produced a mixed layer about the height of the obstacle which was visible as a clear zone for over 100 km. downstream.

Moreover, the ability of islands to block, divert, and dissipate low cloud cover should not be ignored from the standpoint of practical applications. It is enough to note that during World War II, when airfields were established on both sides of Okmok Volcano on Umnak Island in the Aleutians, the field on the downwind side of the Island would consistently remain open under conditions of general low ceilings and visibility.

REFERENCES

1. C. J. Bowley, A. H. Glaser, R. J. Newcomb, and R. Wexler, "Satellite Observations of Wake Formation Beneath an Inversion," *Journal of the Atmospheric Sciences*, vol. 19, No. 1, Jan. 1962, pp. 52-55.
2. K. P. Chopra and L. F. Hubert, "Mesoscale Eddies in the Wake of Islands," *Journal of the Atmospheric Sciences*, vol. 22, No. 6, Nov. 1965, pp. 652-657.
3. A. J. Faller, "Large Eddies in the Atmospheric Boundary Layer and Their Probable Role in the Formation of Cloud Rows," *Journal of the Atmospheric Sciences*, vol. 22, No. 2, Mar. 1965, pp. 176-184.
4. J. Förchtgott, "Vlnové Proudění v Závětrí Horských Hřebenů" [Wave Streaming in the Lee of Mountain Ridges], *Meteorologické Zprávy Praha* [Meteorological Bulletin of Czechoslovakia], vol. 3, No. 3, Oct. 1949, p. 49-51.
5. T. Fujita, "A Technique for Precise Analysis for Satellite Data: Volume I-Photogrammetry," *Meteorological Satellite Laboratory Report No. 14*, U.S. Weather Bureau, Washington, D.C., 1963, 106 pp.

6. T. Fujita, "Use of TIROS Pictures for Studies of the Internal Structure of Tropical Storms," *Research Paper* No. 25, Satellite and Mesometeorology Research Project, Department of Geophysical Sciences, University of Chicago, 1963, 20 pp.
7. T. Fujita, "The Scanning Printer and its Application to Detailed Analysis of Satellite Radiation Data," *Research Paper* No. 34, Satellite and Mesometeorology Research Project, Department of Geophysical Sciences, University of Chicago, 1964, 29 pp.
8. G. L. Heffter, "The Variations of Horizontal Diffusion Parameters and Travel Periods of One Hour or Longer," *Journal of Applied Meteorology*, vol. 4, No. 1, Feb. 1965, pp. 153-156.
9. L. F. Hubert, "Mesoscale Cellular Convection," *Meteorological Satellite Laboratory Report* No. 37, U.S. Weather Bureau, Washington, D.C., 1966, 68 pp.
10. L. F. Hubert and A. F. Krueger, "Satellite Pictures of Mesoscale Eddies," *Monthly Weather Review*, vol. 90, No. 11, Nov. 1962, pp. 457-463.
11. T. W. Kao, "The Phenomena of Blocking in Stratified Flows," *Journal of Geophysical Research*, vol. 70, No. 4, Feb. 15, 1965, pp. 815-822.
12. A. F. Krueger and S. Fritz, "Cellular Cloud Patterns Revealed by TIROS I," *Tellus*, vol. 12, No. 1, Feb. 1961, pp. 1-7.
13. C. C. Lin, "On Periodically Oscillating Wakes in the Oseen Approximation," *Studies in Fluid Mechanics Presented to R. von Mises*, Academic Press, New York, 1959, pp. 170-176.
14. R. R. Long, "Some Aspects of the Flow of Stratified Fluids: II. Experiments of a Two-Fluid System," *Tellus*, vol. 6, No. 1, Feb. 1954, pp. 97-115.
15. R. R. Long, "Some Aspects of the Flow of Stratified Fluids: III. Continuous Density Gradients," *Tellus*, vol. 7, No. 3, Aug. 1955, pp. 341-357.
16. M. Neiburger, "Reflection, Absorption, and Transmission of Insolation by Stratus Clouds," *Journal of Meteorology*, vol. 6, No. 1, Jan. 1949, pp. 98-104.
17. T. Ogata and Y. Tamura, "The Sea Fog Over the Open Sea," *Journal of Meteorological Research*, Tokyo, vol. 7, No. 9, Sept. 1955, pp. 633-642.
18. R. S. Scorer, "Theory of Waves in the Lee of Mountains," *Quarterly Journal of the Royal Meteorological Society*, vol. 75, No. 323, Jan. 1949, pp. 41-56.
19. R. S. Scorer, "Theory of Airflow Over Mountains: IV. Separation of Airflow From the Surface," *Quarterly Journal of the Royal Meteorological Society*, vol. 81, No. 349, July 1955, pp. 340-350.
20. R. S. Scorer, "Airflow Over an Isolated Hill," *Quarterly Journal of the Royal Meteorological Society*, vol. 82, No. 351, Jan. 1956, pp. 75-81.
21. W. K. Widger, P. E. Sherr, and C. W. C. Rogers, "Practical Interpretation of Meteorological Satellite Data," *Technical Report* No. 185, Air Weather Service, 1964, 380 pp.
22. A. I. Voskresensky and L. T. Matveev, "Vodnost i Tubulentnyi Rezhim Sloistoobraznykh Oblakov Arktiki" [Liquid-Water Content and Turbulent Regime of the Arctic Layering Clouds] *Meteorologiya i Gidrologiya* Moskva, No. 11, Nov. 1960, pp. 14-19.

[Received September 21, 1967; revised December 4, 1967]